



## Silver-modulated SiO<sub>2</sub>-supported copper catalysts for selective hydrogenation of dimethyl oxalate to ethylene glycol



Ying Huang<sup>a</sup>, Hiroko Ariga<sup>b</sup>, Xinlei Zheng<sup>a</sup>, Xinping Duan<sup>a</sup>, Satoru Takakusagi<sup>b</sup>, Kiyotaka Asakura<sup>b,\*</sup>, Youzhu Yuan<sup>a,\*</sup>

<sup>a</sup>State Key Laboratory of Physical Chemistry of Solid Surfaces and National Engineering Laboratory for Green Chemical Production of Alcohols-Ethers-Esters, College of Chemistry and Chemical Engineering, Xiamen University, Xiamen 361005, China

<sup>b</sup>Catalysis Research Center, Hokkaido University, Kita-ku N21W10, Sapporo, Hokkaido 001-0021, Japan

### ARTICLE INFO

#### Article history:

Received 12 May 2013

Revised 3 July 2013

Accepted 8 July 2013

#### Keywords:

Copper

Silver

Hydrogenation

Dimethyl oxalate

Ethylene glycol

### ABSTRACT

We present the application of a one-step urea-assisted gelation method to prepare a SiO<sub>2</sub>-supported bimetallic catalyst composed of copper (Cu) and silver (Ag). Results show the remarkably enhanced performance of the catalyst for selective hydrogenation of dimethyl oxalate (DMO) to ethylene glycol (EG). Coupled with a series of characterization and kinetic studies, the improved activity is attributed to the formation of Cu nanoparticles containing Ag nanoclusters on the SiO<sub>2</sub> surface. The coherent interactions between the Cu and Ag species help create the active Cu<sup>+</sup>/Cu<sup>0</sup> species in a suitable proportion and prevent the transmigration of bimetallic nanoparticles during the hydrogenation process. The optimized Cu–Ag/SiO<sub>2</sub> catalyst with an Ag/Cu atomic ratio of 0.05 has a balanced Cu<sup>+</sup>/Cu<sup>0</sup> ratio and highly dispersed bimetal particles, which account for its high turnover frequency, EG selectivity of 97.0%, and excellent catalytic stability during the hydrogenation of DMO to EG for longer than 150 h.

© 2013 Elsevier Inc. All rights reserved.

### 1. Introduction

Ethylene glycol (EG) is widely used as an antifreezing agent, a component of polyester fiber, and a solvent, among others [1]. Given the limited availability of crude oil resources and the increasing demand for EG, novel approaches for the synthesis of EG are being studied to substitute the production of EG derived from traditional petroleum [2,3]. The relatively green and economical coal to EG (CTE) method is one possible alternative. The CTE process involves the gasification of coal to syngas, followed by the coupling of CO with nitrite esters to oxalates and the subsequent hydrogenation of oxalates to EG [1,4,5]. The selective hydrogenation of dimethyl oxalate (DMO) to EG is one of the key reactions in the CTE route that has drawn much attention. Several problems remain unsolved despite considerable efforts in the study of DMO hydrogenation process. To date, EG selectivity and catalytic stability still need improvement, the interaction with active sites remain controversial, and the process of catalyst deactivation requires further elucidation. A deeper understanding of the generic concepts is necessary for more rational catalyst design.

The Cu-based catalysts have been studied extensively in the vapor-phase hydrogenation of DMO. Cu-based catalysts allow for the selective hydrogenation of carbon–oxygen bonds, while remaining relatively inactive during carbon–carbon bond hydrogenolysis [6]. To date, Cu–Cr catalysts remain the preferred industrial catalysts for CTE because of their relatively high catalytic activity and durability [7–9]. Unfortunately, these catalysts require the use of toxic chromium, which could endanger the safety of the environment and the industrial workers. Therefore, different alternative carriers (e.g., SiO<sub>2</sub>, Al<sub>2</sub>O<sub>3</sub>, and ZnO) were evaluated for the synthesis of Cr-free Cu-based catalysts [10–12]. Among these carriers, the Cu/SiO<sub>2</sub> catalyst had the highest EG yield. Thus, the Cu/SiO<sub>2</sub> catalyst was considered a potential alternative for the conventional Cu–Cr catalyst. However, the Cu/SiO<sub>2</sub> catalyst is relatively non-resistant to sintering and is mechanically unstable for industrial operation [6,13–16]. Thus, considerable effort has focused on modifying the Cu/SiO<sub>2</sub> catalyst using various methods, including the addition of a second species [13–16], adoption of different preparation methods [3,17–21], and use of different silica structures for support [22–26]. Cu, Ag, and Au are coinage metals belonging in the same group in the periodic table. These metals possess a face-centered cubic (fcc) structure, with close lattice parameters. In addition, these metals have similar electronic structures and physical chemical properties. These metals can also form intermetallic or alloy phases with each other. The synergistic effects between the Cu–Au [27,28], Cu–Ag [29,30], and Au–Ag [31,32] bimetallic catalysts

\* Corresponding authors. Fax: +81 11 706 9113 (K. Asakura), +86 592 2183047 (Y. Yuan).

E-mail addresses: [askr@cat.hokudai.ac.jp](mailto:askr@cat.hokudai.ac.jp) (K. Asakura), [yzyuan@xmu.edu.cn](mailto:yzyuan@xmu.edu.cn) (Y. Yuan).

have been previously reported. Recent results showed that a bimetallic Cu–Au catalyst with a large amount of Au could improve catalyst performance during the hydrogenation of DMO to MG [33]. By contrast, a catalyst with a small amount of Au exhibited remarkably enhanced activity and stability during the hydrogenation of DMO to EG [34]. Spectroscopic studies revealed that the Cu–Au alloy nanoparticles (NPs) were formed on the catalyst surfaces, which were believed to retard the surface transmigration of Cu species during hydrogenation. Furthermore, the ratio of surface Cu<sup>+</sup> and Cu<sup>0</sup> would vary, based on the amount of incorporated Au. Consequently, different catalytic behaviors would be observed under similar conditions. The catalytic performance of the Cu–Ag/SiO<sub>2</sub> catalysts prepared by a deposition–precipitation method has been evaluated for the DMO hydrogenation reaction, with MG as the main product [35]. However, the structure and structure–activity relationships of these Cu–Ag catalysts remain ambiguous.

In this work, we incorporate a small amount of Ag into Cu/SiO<sub>2</sub> using a urea-assisted gelation method. Additionally, we found that the bimetallic Cu–Ag/SiO<sub>2</sub> catalysts could efficiently promote the hydrogenation of DMO to EG. Kinetic and spectroscopic studies show that an intimate interaction between Cu and Ag NPs, as well as a cooperative effect between these, might be essentially responsible for the observed enhanced catalysis.

## 2. Experimental

### 2.1. Catalyst preparation

The bimetallic Cu–Ag/SiO<sub>2</sub> catalysts with a preset metal loading of 10 wt% were prepared using a urea-assisted gelation method [13]. Briefly, 4.5 g of 40 wt% LudoxAS-40 colloidal silica was dispersed in a 100 mL aqueous solution containing 6.0 g of urea, a known amount of AgNO<sub>3</sub>, Cu(NO<sub>3</sub>)<sub>2</sub>·3H<sub>2</sub>O, and aqueous ammonia (28 wt%) in a round-bottomed flask. The suspension was vigorously stirred at 353 K in an oil bath for 4 h. The obtained precipitate was separated by hot filtration, washed thrice with deionized water, dried at 393 K overnight, and calcinated at 623 K for 4 h. The catalyst precursor was denoted as Cu<sub>1</sub>–Ag<sub>x</sub>/SiO<sub>2</sub>, where *x* represents the atomic ratio of Ag and Cu.

A Cu/SiO<sub>2</sub> catalyst with 10 wt% Cu and an Ag/SiO<sub>2</sub> catalyst with 10 wt% Ag were similarly prepared using a urea-assisted gelation method.

### 2.2. Catalyst characterizations

The N<sub>2</sub> adsorption–desorption isotherms for the catalysts were measured at 77 K using a Micromeritics TriStar II 3020 porosimetry analyzer. The samples were degassed at 573 K for 3 h prior to the measurements. The specific surface area (*S*<sub>BET</sub>) was calculated using the Brunauer–Emmett–Teller (BET) method, which adopted the isotherm data in a relative pressure (*P*/*P*<sub>0</sub>) range of 0.05–0.2. The mesopore size distributions were evaluated from the desorption branch of the isotherm using the Barrett–Joyner–Halenda (BJH) method. The total pore volume depended on the adsorbed N<sub>2</sub> volume at a relative pressure of approximately 0.99.

X-ray diffraction (XRD) patterns for the catalyst samples were obtained on a PANalytical X'pert Pro Super X-ray diffractometer using Cu Kα radiation ( $\lambda = 0.15418$  nm) with a scanning angle ( $2\theta$ ) ranging from 10° to 90°, tube voltage of 40 kV, and a current of 30 mA. For the *in situ* XRD measurements, a 5% H<sub>2</sub>–95% N<sub>2</sub> mixture was introduced to the system at a flow rate of 50 mL min<sup>-1</sup>. Temperature ramping programs were performed at room temperature as well as at 523, 573, 623, 673, 723, 773, 873, and 973 K, with a rate of 2 K min<sup>-1</sup>. The XRD patterns were collected after

samples reached the preset temperatures for 30 min. Each diffraction pattern was identified by matching the results with reference patterns included in the JCPDS data base. The full-width-at-half-maximum of Cu (1 1 1) diffraction at a  $2\theta$  of 43.2° was used to calculate the Cu crystallite size using the Scherrer equation.

The hydrogen-temperature-programmed reduction (H<sub>2</sub>-TPR) for the as-calcined catalyst samples was carried out on a Micromeritics Autochem II 2920 instrument connected to a Hiden Qic-20 mass spectrometer (MS). A quartz U-tube was loaded with 100 mg of the calcined catalyst and dried in an argon stream at 393 K for 1 h. After cooling the catalysts to room temperature under an argon atmosphere, a flow of 5% H<sub>2</sub>–95% N<sub>2</sub> (50 mL min<sup>-1</sup>) was fed into the catalyst bed. The temperature was then ramped linearly from the ambient temperature to 1073 K, at a rate of 10 K min<sup>-1</sup>. A 5A zeolite trap was connected to the reactor outlet to remove any moisture. The hydrogen consumption was simultaneously monitored by a thermal conductivity detector (TCD) and MS.

Transmission electron microscopy (TEM) images were obtained using a Tecnai F30 apparatus operated at 300 kV. The composition analysis of each metal particle was performed using energy-dispersive X-ray spectroscopy (EDS) at scanning TEM (STEM) mode. The powdered catalyst was dispersed in ethanol using ultrasound at room temperature. The as-obtained solution was then dropped into the carbon-coated molybdenum grids.

Ultraviolet–visible light (UV–vis) diffuse reflectance spectroscopy (DRS) of the as-reduced catalysts was collected using a UV–vis–NIR Cary 5000 scanning spectrophotometer. All catalyst precursors were freshly reduced in a 5% H<sub>2</sub>–95% N<sub>2</sub> atmosphere at 623 K for 4 h. The as-reduced samples were carefully collected under an argon atmosphere at room temperature and sealed in glass bottles before the UV–vis DRS measurements.

The Cu and Ag K-edge XAFS measurements were performed using the transmission mode at the BL12C and NW10 beam line of the PF-AR and Photon Factory, Institute of Materials Structure Science, High Energy Accelerator Research Organization (IMSS-KEK), Japan (Proposal Nos. 2012G680 and 2012G644). The storage ring was operated at 2.5 GeV and 450 mA using the top-up mode. A Si (1 1 1) double crystal monochromator was used in the quick scan mode. After reduction under 5% H<sub>2</sub>–95% Ar at 623 K for 2 h, the samples were sealed in glass cells under He (Cu) or Ar (Ag). The XAFS spectra were then obtained at room temperature. The EXAFS analysis was performed using the REX (version 2.5) program (Rigaku). The Fourier transformation of the *k*<sup>3</sup>-weighted EXAFS oscillation from the *k* space to the *r* space was performed over the range of 30–140 nm<sup>-1</sup> to obtain a radial distribution function. The inversely filtered Fourier data were analyzed using a non-linear least squares curve fitting method in the *k* range of 30–140 nm<sup>-1</sup>. For the curve fitting analysis, the phase shift and amplitude functions of the Ag–Cu, Ag–Ag, and Ag–O shells were calculated using the FEFF program.

X-ray photoelectron spectroscopy (XPS) and Auger electron spectroscopy (XAES) were performed using a JPS-9010MC photoelectron spectrometer equipped with an Al Kα X-ray radiation source (*hν* = 1486.6 eV). Prior to the measurements, each sample was pressed into a thin disk and pretreated in an atmosphere of 5% H<sub>2</sub>–95% Ar ( $5 \times 10^4$  Pa) at 623 K for 1 h in an auxiliary pretreatment chamber. After the pretreatment, the sample was introduced into the XPS chamber to avoid exposure to air. The XPS spectra of as-calcined and pretreated samples were recorded at room temperature. The binding energy (BE) was calibrated using C 1s peak at 284.6 eV as reference with an uncertainty of ±0.2 eV.

The Cu dispersion in each catalyst was determined by dissociative N<sub>2</sub>O chemisorption and hydrogen pulse reduction using a Micromeritics Autochem II 2920 apparatus with a TCD. Typically, 100 mg of Cu/SiO<sub>2</sub> was calcined at 623 K, reduced in 5% H<sub>2</sub>–95% N<sub>2</sub> (50 mL min<sup>-1</sup>) at 623 K for 4 h, and cooled to 333 K. Pure N<sub>2</sub>O

(30 mL min<sup>-1</sup>) was then introduced for 30 min to completely oxidize the surface Cu atoms into Cu<sub>2</sub>O. The hydrogen pulse reduction of the surface Cu<sub>2</sub>O to metallic Cu was conducted at 573 K to ensure that the chemisorbed oxygen could immediately react with the high-purity hydrogen supplied from a 0.4 mL loop. Excess moisture was removed using a 5A zeolite dehydration trap. Hydrogen pulse-dosing was repeated until the pulse area remained constant. The consumed amount of hydrogen was obtained by subtracting the area of the first few pulses from the area of the other pulses. The Cu loading of all the reduced catalysts was analyzed by inductively coupled plasma optical emission spectrometry (ICP-OES) using a Thermo Electron IRIS Intrepid II XSP. The Cu dispersion was calculated by dividing the amount of chemisorption sites by the total number of supported Cu atoms per gram of the catalyst.

### 2.3. Catalytic testing

The catalytic performance for DMO hydrogenation was evaluated using a fixed-bed microreactor equipped with a computer-controlled auto-sampling system. Typically, 200 mg of the catalyst precursor (40–60 meshes) was loaded into the center of the reactor, with both sides of the catalyst bed packed with quartz powder (40–60 meshes). The catalyst was activated under a 5% H<sub>2</sub>–95% N<sub>2</sub> flow (50 mL min<sup>-1</sup>) at 623 K for 4 h, with a ramping rate of 2 K min<sup>-1</sup>. The catalyst was cooled to the desired reaction temperature, and pure H<sub>2</sub> (99.999%) was allowed to pass through the catalyst bed. A DMO methanol solution (0.01 g mL<sup>-1</sup>) was then pumped into the reactor using a Series III digital HPLC pump (Scientific Systems, Inc.) with a system pressure of 3.0 MPa. The outlet stream was sampled using an automatic Valco 6-ports valve system and analyzed using an online gas chromatograph (GC9790 Gas Chromatograph, Zhe Jiang Fu Li Analytical Instrument Co., Ltd.) with a flame ionization detector and a KB-Wax capillary column (30 m × 0.45 mm × 0.85 μm) at intervals of 30 min.

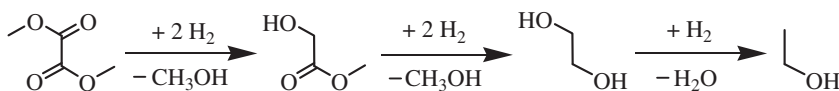
The initial turn over frequency (TOF) of the reaction was measured when the DMO conversion was lower than 35%. The TOF value was based on the Cu dispersion or the number of surface metal atoms estimated by the metal dispersion, according to an equation in the literature [36]. This value indicated the moles of DMO converted per hour by each mole of the metal on the catalyst surface (mol<sub>DMO</sub> mol<sub>metal (surf)</sub><sup>-1</sup> h<sup>-1</sup> or simply h<sup>-1</sup>).

## 3. Results and discussion

### 3.1. Catalytic activity and stability

Vapor-phase DMO hydrogenation is known to comprise several continuous reactions (Scheme 1), including DMO hydrogenation to methyl glycolate (MG), MG hydrogenation to EG, and deep hydrogenation of EG to ethanol (EtOH). Moreover, by-products of 1,2-butanediol (1,2-BDO) and 1,2-propanediol (1,2-PDO) are also produced as a result of the dehydration reaction between EG and EtOH or methanol [1,16]. To rigorously compare the catalytic activity between Cu/SiO<sub>2</sub> and Cu<sub>1</sub>–Ag<sub>x</sub>/SiO<sub>2</sub>, the DMO conversion was limited to less than 35% by adjusting the DMO weight liquid hourly space velocity (WLHSV<sub>DMO</sub>). The DMO conversion data were then used to calculate the TOF according to the Cu dispersion (TOF<sub>Cu</sub>) and total metal dispersion (TOF<sub>M</sub>), as listed in Table 1. The TOF<sub>Cu</sub> exhibited volcano-type improvement with the increasing Ag content in Cu<sub>1</sub>–Ag<sub>x</sub>/SiO<sub>2</sub>, which reached its maximum value (18.3 h<sup>-1</sup>) with the Ag/Cu atomic ratio of 0.05:1. The trends in the TOF<sub>M</sub> of the catalysts were similar to those exhibited by TOF<sub>Cu</sub>. However, the value of TOF<sub>M</sub> was slightly higher, as compared with TOF<sub>Cu</sub> when the Ag/Cu atomic ratio was below 0.1. Therefore, several interactions must have occurred between Ag and Cu. Further increasing the Ag loading restrained the catalytic activity. Additionally, this restriction was more evident when the monometallic Ag catalyst was taken into consideration. The results demonstrated the synergistic effect between Cu and Ag during the hydrogenation of DMO to EG.

DMO hydrogenation was conducted at 463 K under a WLHSV<sub>DMO</sub> of 1.05 h<sup>-1</sup>, a H<sub>2</sub> pressure of 3.0 MPa, and a H<sub>2</sub>/DMO molar ratio of 80. The resulting bimetallic catalysts had more than 97% DMO conversion (Table S1 in the Supporting information). However, the Cu/SiO<sub>2</sub> catalyst demonstrated 87.2% DMO conversion and 30.7% selectivity to EG, whereas the Ag/SiO<sub>2</sub> catalyst was almost inactive. That is, Ag incorporated with Cu/SiO<sub>2</sub> could dramatically improve the EG yield, as compared with the monometallic Cu/SiO<sub>2</sub> or Ag/SiO<sub>2</sub>. The Ag/Cu atomic ratio had a notably significant effect on tuning the catalytic capability of DMO hydrogenation. Introducing a very small amount of Ag (Ag/Cu atomic ratio, 0.02; Ag loading, 0.26 wt%) in the Cu/SiO<sub>2</sub> catalyst increased the EG yield to 58.4%, which was twice as that of the monometallic Cu/SiO<sub>2</sub> catalyst. By increasing the Ag/Cu atomic



Scheme 1. Reaction pathway for the hydrogenation of DMO to MG, EG, and EtOH.

Table 1  
TOF of Cu<sub>1</sub>–Ag<sub>x</sub>/SiO<sub>2</sub> catalysts for DMO hydrogenation.<sup>a</sup>

| Catalyst  | Conversion (%) | Selectivity (%) |      | TOF <sub>Cu</sub> <sup>b</sup> (h <sup>-1</sup> ) | TOF <sub>M</sub> <sup>c</sup> (h <sup>-1</sup> ) |
|---|----------------|-----------------|------|---|--|
|   |                | EG              | MG   |   |  |
| Cu/SiO <sub>2</sub>                                   | 16.0           | 4.8             | 95.2 | 10.1  | 11.3   |
| Cu <sub>1</sub> –Ag <sub>0.02</sub> /SiO <sub>2</sub> | 22.3           | 8.2             | 91.8 | 13.5  | 15.1   |
| Cu <sub>1</sub> –Ag <sub>0.05</sub> /SiO <sub>2</sub> | 33.8           | 8.8             | 91.2 | 18.3  | 20.6   |
| Cu <sub>1</sub> –Ag <sub>0.1</sub> /SiO <sub>2</sub>  | 24.5           | 8.1             | 91.9 | 16.1  | 16.0   |
| Cu <sub>1</sub> –Ag <sub>0.2</sub> /SiO <sub>2</sub>  | 16.4           | 5.1             | 94.9 | 13.3  | 12.1   |
| Ag/SiO <sub>2</sub> <sup>d</sup>                      | 3.7            | 1.6             | 98.4 | –   | 5.5  |

<sup>a</sup> Reaction conditions: *T* = 463 K, *P*(H<sub>2</sub>) = 3.0 MPa, H<sub>2</sub>/DMO molar ratio = 80, WLHSV<sub>DMO</sub> = 3.6 h<sup>-1</sup>.

<sup>b</sup> TOF<sub>Cu</sub> was calculated by Cu dispersion.

<sup>c</sup> TOF<sub>M</sub> was calculated by metal dispersion.

<sup>d</sup> WLHSV<sub>DMO</sub> = 1.05 h<sup>-1</sup>.

ratio to 0.05, the catalyst produced the maximum EG yield of 85.9%. However, when the Ag/Cu atomic ratio was further increased to 0.1, the catalyst had a lower EG yield.

The catalytic performance of the Cu/SiO<sub>2</sub> and optimized Cu<sub>1</sub>-Ag<sub>0.05</sub>/SiO<sub>2</sub> catalysts were further investigated under different WLHSV<sub>DMO</sub> values (Fig. 1). The conversion of DMO over the Cu<sub>1</sub>-Ag<sub>0.05</sub>/SiO<sub>2</sub> catalyst remained higher than 99% when the WLHSV<sub>DMO</sub> varied from 0.3 h<sup>-1</sup> to 1.05 h<sup>-1</sup>. Subsequently, the conversion over Cu/SiO<sub>2</sub> began to decline when WLHSV<sub>DMO</sub> was set at 0.6 h<sup>-1</sup>. At a set of WLHSV<sub>DMO</sub> ranged from 0.3 h<sup>-1</sup> to 0.75 h<sup>-1</sup>, the selectivity to EG was approximately 97% over the Cu<sub>1</sub>-Ag<sub>0.05</sub>/SiO<sub>2</sub> catalyst while the selectivity to MG and other by-products (EtOH, 1,2-PDO, and 1,2-BDO) were lower than 1% and 2%, respectively. However, the selectivity to EG over the Cu/SiO<sub>2</sub> was lower than 50% and MG as the partial hydrogenation product became dominant when the WLHSV<sub>DMO</sub> reached 0.75 h<sup>-1</sup>. In this case, the selectivity to MG was 43.2% and almost no other by-products were yielded over the Cu/SiO<sub>2</sub> catalyst. Further increasing the WLHSV<sub>DMO</sub>, the selectivity to EG over the Cu<sub>1</sub>-Ag<sub>0.05</sub>/SiO<sub>2</sub> catalyst was also decreased, accompanying with the increase in selectivity to MG and suppression of excess hydrogenation or dehydration products. The EG yield over Cu<sub>1</sub>-Ag<sub>x</sub>/SiO<sub>2</sub> catalysts was clearly a function of WLHSV<sub>DMO</sub> (Fig. S1 in the Supporting information) and easy to obtain, thereby indicating the significant influence of the WLHSV<sub>DMO</sub>. Better catalytic performance with higher tolerance to WLHSV<sub>DMO</sub> was observed with the bimetallic Cu–Ag/SiO<sub>2</sub> catalysts for the hydrogenation of DMO, as compared with the Cu/SiO<sub>2</sub> catalyst.

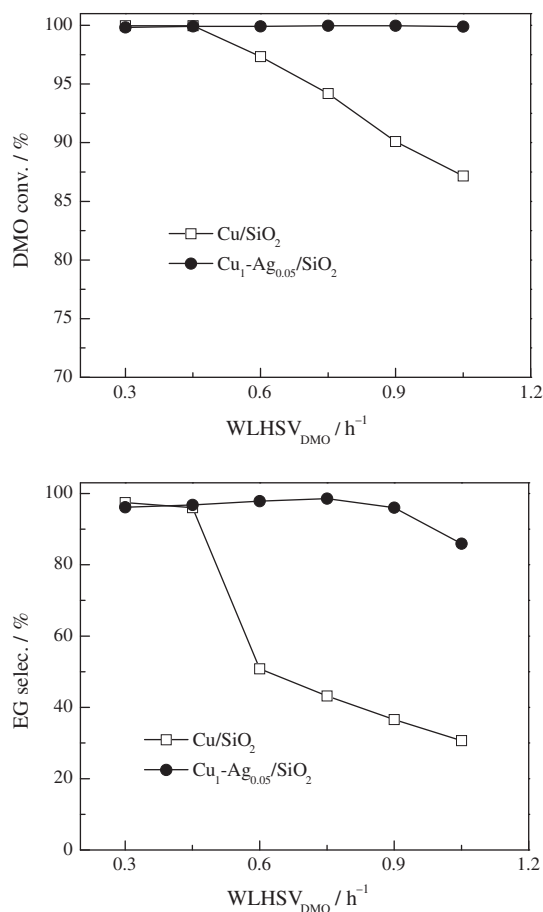


**Fig. 1.** DMO hydrogenation over Cu/SiO<sub>2</sub> and Cu<sub>1</sub>-Ag<sub>0.05</sub>/SiO<sub>2</sub> catalysts as a function of WLHSV<sub>DMO</sub>. Reaction conditions:  $T = 463$  K,  $P(\text{H}_2) = 3.0$  MPa,  $\text{H}_2/\text{DMO}$  molar ratio = 80.

The long-term catalytic behaviors of the Cu/SiO<sub>2</sub> and optimized Cu<sub>1</sub>-Ag<sub>0.05</sub>/SiO<sub>2</sub> catalysts were further evaluated at 463 K and 3.0 MPa under a H<sub>2</sub>/DMO molar ratio of 80 and a WLHSV<sub>DMO</sub> of 0.6 h<sup>-1</sup>. The DMO conversion and EG selectivity of the Cu/SiO<sub>2</sub> catalyst dramatically decreased after 100 h to approximately 60% and 10%, respectively (Fig. 2), whereas the Cu<sub>1</sub>-Ag<sub>0.05</sub>/SiO<sub>2</sub> catalyst retained its initial activity even after more than 150 h. These results suggested that adding the proper amount of Ag to the Cu/SiO<sub>2</sub> catalyst can remarkably enhance DMO hydrogenation and effectively improve catalyst stability.

### 3.2. Catalyst characterizations

#### 3.2.1. Physicochemical properties of the catalysts

The metal loadings of the catalysts were determined using ICP-OES, as listed in Table 2. The actual loadings of Cu and Ag were slightly lower, as compared with the theoretical value. This difference occurred because the weakly absorbed metallic ions on the silica gel were eluted during the filtration process. However, the actual atomic ratio of Ag/Cu in the catalysts was close to the preset value. The physicochemical properties of the catalysts are summarized in Table 2. The introduction of Ag had no obvious effect on the surface area of the catalysts, whereas the pore volume and average pore diameter were slightly increased when the Ag/Cu atomic ratios were lower than 0.1. The values then decreased after further introduction of Ag. The concurrent oxidation of metallic Ag species while determining the Cu dispersion by N<sub>2</sub>O at 333 K was ignored because the reaction of N<sub>2</sub>O with the metallic Ag species occurs at a relatively high temperature (658 K) [37] or requires long reaction times (5 h) when the temperature is below 373 K [38]. In addition, this phenomenon occurs when the Ag content was very low in the bimetallic catalysts. The Cu dispersion of the bimetallic Cu–Ag/SiO<sub>2</sub> catalysts is summarized in Table 2. This dispersion initially increased and reached its maximum at an Ag/Cu atomic ratio of 0.05, with a value of 43.1 m<sup>2</sup> g<sup>-1</sup>. The Cu dispersion then gradually decreased with the further increase in Ag loading. The results suggested that the introduction of the proper amount of Ag facilitated the higher dispersion of Cu particles. The Cu<sub>1</sub>-Ag<sub>0.05</sub>/SiO<sub>2</sub> had the highest Cu dispersion and notably presented the optimal catalytic performance under identical reaction conditions.

#### 3.2.2. TEM, EDS and XRD

The morphologies and structural details of the bimetallic catalysts were examined using TEM (Fig. 3). The metal nanoparticles were distributed uniformly on the surfaces of the silica. The

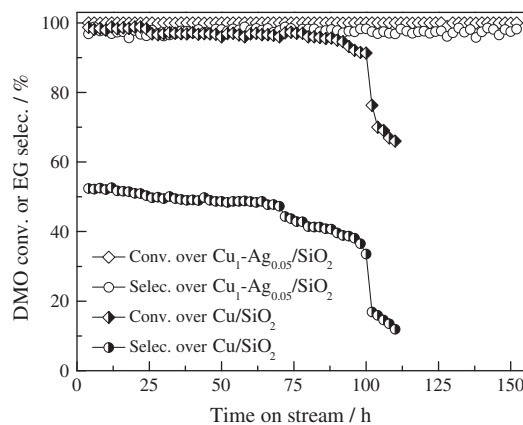


**Fig. 2.** DMO hydrogenation over Cu/SiO<sub>2</sub> and Cu<sub>1</sub>-Ag<sub>0.05</sub>/SiO<sub>2</sub> catalysts as a function of time on stream. Reaction conditions:  $T = 463$  K,  $P(\text{H}_2) = 3.0$  MPa,  $\text{H}_2/\text{DMO}$  molar ratio = 80, WLHSV<sub>DMO</sub> = 0.6 h<sup>-1</sup>.

**Table 2**  
Physicochemical properties of Cu<sub>1</sub>–Ag<sub>x</sub>/SiO<sub>2</sub> catalysts.

| Catalyst  | Content <sup>a</sup> (wt%) |      | Ag/Cu atomic ratio | S <sub>BET</sub> (m <sup>2</sup> g <sup>-1</sup> ) | V <sub>pore</sub> (cm <sup>3</sup> g <sup>-1</sup> ) | D <sub>pore</sub> (nm) | Metal dispersion (%) |        |
|---|----------------------------|------|--------------------|--|--|------------------------|----------------------|--------|
|   | Cu                         | Ag   |                    |  |  |                        | By N <sub>2</sub> O  | By TEM |
| Cu/SiO <sub>2</sub>                                   | 8.7                        | –    | –                  | 225  | 0.82   | 12.5                   | 35.3                 | 31.6   |
| Cu <sub>1</sub> –Ag <sub>0.02</sub> /SiO <sub>2</sub> | 8.3                        | 0.26 | 0.018              | 217  | 0.90   | 13.8                   | 38.6                 | 33.8   |
| Cu <sub>1</sub> –Ag <sub>0.05</sub> /SiO <sub>2</sub> | 7.9                        | 0.65 | 0.048              | 225  | 0.90   | 13.7                   | 43.1                 | 38.4   |
| Cu <sub>1</sub> –Ag <sub>0.1</sub> /SiO <sub>2</sub>  | 7.3                        | 1.2  | 0.097              | 217  | 0.96   | 14.9                   | 40.5                 | 37.2   |
| Cu <sub>1</sub> –Ag <sub>0.2</sub> /SiO <sub>2</sub>  | 6.6                        | 2.0  | 0.18               | 188  | 0.63   | 12.1                   | 36.3                 | 33.8   |
| Ag/SiO <sub>2</sub>                                   | –                          | 9.1  | –                  | 109  | 0.45   | 15.2                   | –                    | 7.1    |
| SiO <sub>2</sub>                                      | –                          | –    | –                  | 108  | 0.34   | 9.9                    | –                    | –      |

<sup>a</sup> Determined by ICP-OES analysis.

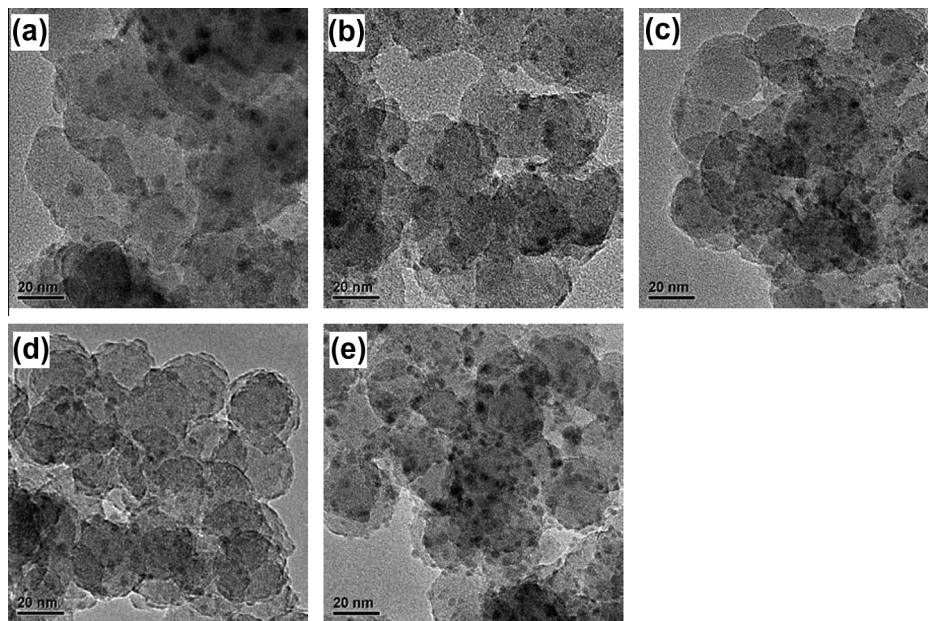


**Fig. 3.** TEM images of as-reduced catalysts. (a) Cu/SiO<sub>2</sub>, (b) Cu<sub>1</sub>–Ag<sub>0.02</sub>/SiO<sub>2</sub>, (c) Cu<sub>1</sub>–Ag<sub>0.05</sub>/SiO<sub>2</sub>, (d) Cu<sub>1</sub>–Ag<sub>0.1</sub>/SiO<sub>2</sub>, and (e) Cu<sub>1</sub>–Ag<sub>0.2</sub>/SiO<sub>2</sub>.

particle diameter distribution showed that mean particle size of all the samples was approximately 3 nm (Fig. S2 in the Supporting information). High-resolution TEM (HRTEM) of a typical metal particle in the Cu<sub>1</sub>–Ag<sub>0.05</sub>/SiO<sub>2</sub> catalyst (Fig. S3 in the Supporting information) indicated that the 0.188 nm interval of lattice fringes was smaller, as compared with those monometallic Ag (111) (0.236 nm), Ag (200) (0.204 nm), and Cu (111) (0.209 nm), but larger than Cu (200) (0.181 nm). This result may indicate the formation of the Cu–Ag alloy after reduction. The total metal dispersion of the catalysts was calculated in accordance with the TEM, as listed in Table 2. The total metal dispersion of the catalysts improved with the increasing Ag/Cu atomic ratio, which agrees with the observed trend of Cu dispersion. The dispersion of the Cu<sub>1</sub>–Ag<sub>0.05</sub>/SiO<sub>2</sub> catalyst reached its maximum at 38.4 m<sup>2</sup> g<sup>-1</sup>.

The high-angle annular dark-field scanning transmission electron microscopy (HAADF-STEM) images of the as-reduced Cu<sub>1</sub>–Ag<sub>x</sub>/SiO<sub>2</sub> bimetallic catalysts were shown in Fig. S4 (in the Supporting information). The tiny bright spots in the images correspond to metal nanoparticles supported on the SiO<sub>2</sub>. In combination with X-ray energy dispersive spectroscopy (X-EDS) system equipped with a sub-nanometer probe, we can locate the convergent electron beam (0.5 nm) at any position of the sample to obtain more detail features of metal nanoparticles such as element distribution and composition under HAADF-STEM mode. The compositions of individual metallic particles on the several as-reduced Cu<sub>1</sub>–Ag<sub>x</sub>/SiO<sub>2</sub> catalysts were measured by the point EDS analysis

on the selected fifteen metal particles. The STEM-EDS results revealed that both Cu and Ag elements were detectable, but the Ag/Cu atomic ratio was higher as compared with the present value in most of the selected metallic particles, particularly when the actual Ag/Cu ratio was higher than 0.05. In other words, segregation of the Ag species could occur in bulk particles.

The XRD patterns showed that the as-calcined catalysts were amorphous, except for the Ag/SiO<sub>2</sub> (Fig. S5 in the Supporting information). The introduction of Ag to the Cu/SiO<sub>2</sub> catalyst did not significantly change the XRD patterns of the catalyst. Neither Cu nor Ag species could be detected in these precursors, thereby implying that Cu and Ag were highly dispersed on the porous silica support by the urea-assisted gelation method. However, well-dispersed pure Ag/SiO<sub>2</sub> catalysts could not be prepared using this method.

We then conducted *in situ* XRD characterization to monitor the phase evolution of the Cu/SiO<sub>2</sub> and optimized Cu<sub>1</sub>–Ag<sub>0.05</sub>/SiO<sub>2</sub> catalysts as the reduction temperature was increased under a 5% H<sub>2</sub>–95% N<sub>2</sub> atmosphere. As shown in Fig. 4, the characteristic peak of Cu (111) (JCPDS 04-0836) at 2θ of 43.2° was detected because several Cu<sup>2+</sup> species on the Cu/SiO<sub>2</sub> catalyst precursor were reduced to Cu<sup>0</sup> when the reduction temperature reached 523 K. According to the Scherrer equation, the Cu crystallite size of the Cu/SiO<sub>2</sub> catalyst was smaller than 4 nm when the reduction temperature was lower than 773 K, whereas the Cu crystallite size of the Cu<sub>1</sub>–Ag<sub>0.05</sub>/SiO<sub>2</sub> catalyst was smaller than 3.2 nm at the same reduction temperature range. The diffraction peaks of the

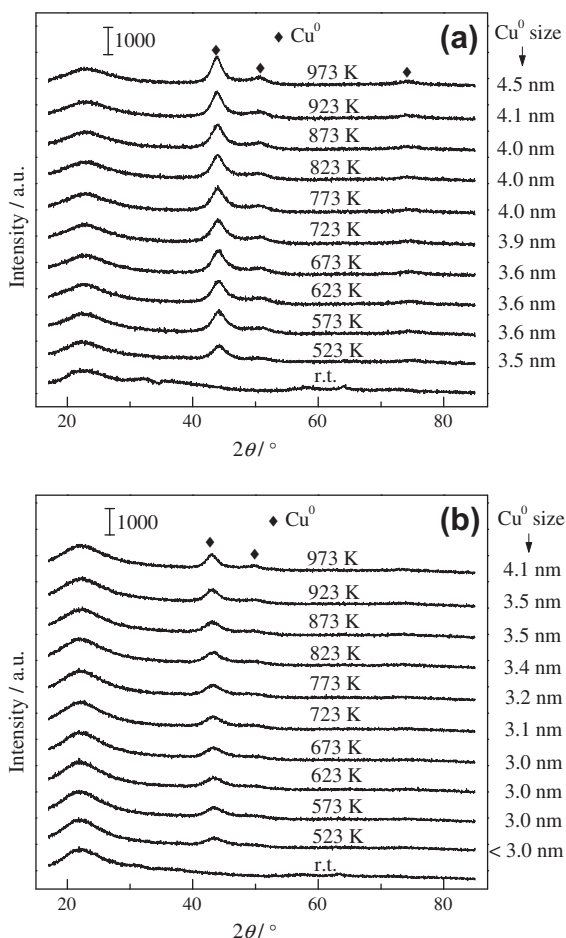


**Fig. 4.** *In situ* XRD patterns of as-calcined catalysts as a function of the reduction temperature under a 5% H<sub>2</sub>–95% N<sub>2</sub> atmosphere. (a) Cu/SiO<sub>2</sub> and (b) Cu<sub>1</sub>–Ag<sub>0.05</sub>/SiO<sub>2</sub>.

Cu<sub>1</sub>–Ag<sub>0.05</sub>/SiO<sub>2</sub> catalyst were, to some extent, broader than those of the pure Cu catalyst. Therefore, adding the proper amount of Ag to the Cu/SiO<sub>2</sub> catalyst could improve the Cu dispersion. This observation was in accordance with the results of the dissociative N<sub>2</sub>O chemisorption and TEM. When the reduction temperature under the 5% H<sub>2</sub>–95% N<sub>2</sub> flow is further increased, the Cu diffraction peaks of Cu/SiO<sub>2</sub> and Cu<sub>1</sub>–Ag<sub>0.05</sub>/SiO<sub>2</sub> become sharper. Thus, similar phase evolution behavior is observed in both catalysts.

After a long-term catalytic test, the catalysts were carefully collected under a hydrogen atmosphere at room temperature and sealed in glass bottles to protect the samples from oxidation. The XRD diffraction peaks of the metallic copper in the Cu/SiO<sub>2</sub> and Cu<sub>1</sub>–Ag<sub>0.05</sub>/SiO<sub>2</sub> catalysts were significantly different from each other (Fig. S6 in the Supporting information). The Cu diffraction peak of the spent Cu/SiO<sub>2</sub> catalyst at 2θ of 43.2° was sharper, as compared with that of the Cu<sub>1</sub>–Ag<sub>0.05</sub>/SiO<sub>2</sub> catalyst. The changes in the Cu<sub>1</sub>–Ag<sub>0.05</sub>/SiO<sub>2</sub> catalyst before and after the long-term reaction were not significant. Furthermore, the TEM images of these catalysts revealed consistent results (Fig. S7 in the Supporting information). The transmigration and aggregation of Cu occurred on the Cu/SiO<sub>2</sub> catalyst after the long-term reaction. Thus, we speculated that Cu agglomeration was one of the key factors that caused the deactivation of the catalyst. The addition of Ag was clearly important for retarding the aggregation of the metallic Cu crystallites.

### 3.2.3. H<sub>2</sub>-TPR

In several cases, the presence of a noble metal affected the reducibility of the surface metal oxides. The H<sub>2</sub>-TPR characterizations

were performed to investigate the reducibility of the as-calcined samples with different Ag/Cu atomic ratios. A reduction peak for the as-calcined Ag/SiO<sub>2</sub> catalyst was not obvious (Fig. S8 in the Supporting information). The as-calcined Cu/SiO<sub>2</sub> presented a reduction peak at 518 K, which was assigned to the reduction of highly dispersed CuO to Cu<sup>0</sup> and copper phyllosilicate to Cu<sup>+</sup> [3,39]. The reduction peaks of the bimetallic samples gradually shifted to a lower value with the increasing Ag/Cu atomic ratio. The introduction of Ag had the tendency to decrease the reduction temperature, which was consistent with the results of Zhou et al. [30]. These results suggest that several significant interactions occurred between the Cu and Ag species.

### 3.2.4. UV–vis DRS

UV–vis DRS of the as-reduced Ag/SiO<sub>2</sub> catalyst had a strong absorption peak at 395 nm, which is typical for the well-known surface plasmon resonance (SPR) band of Ag NPs (Fig. S9 in the Supporting information). Meanwhile, Cu/SiO<sub>2</sub> showed a very weak and broad SPR band at approximately 600 nm. The UV–vis DRS spectra of the bimetallic catalysts produced a single SPR band between 400 nm and 600 nm, thereby revealing that it was not a physical mixture of the individual metals [40]. The increasing Ag/Cu atomic ratio gradually shifted the SPR band into the blue range. Therefore, the electronic structure of the bimetallic samples changed after the introduction of Ag. This change occurred because the SPR bands of the metal particles are produced by the collective oscillations of the conduction electrons. The d-band energy level continuously changed because of the increasing amount of Ag [40,41].

### 3.2.5. XPS and XAES

XPS was employed to investigate the surface valence state of the as-reduced Cu–Ag/SiO<sub>2</sub> catalysts. For the Cu/SiO<sub>2</sub> catalyst, the Cu 2p XPS peaks corresponding to Cu 2p<sub>3/2</sub> and Cu 2p<sub>1/2</sub> appeared at 932.5 eV and 952.4 eV, respectively (Fig. S10 in the Supporting information). Nevertheless, the BE of Cu 2p<sub>3/2</sub> was shifted to higher values with the increasing Ag content, thereby indicating that the electronic effect was more obvious. The absence of the 2d → 3d satellite peaks at 934.9 or 933.5 eV suggested that Cu<sup>2+</sup> was successfully reduced to Cu<sup>0</sup> and/or Cu<sup>+</sup> after reduction at 623 K [13].

The Ag 3d XPS spectra of the as-reduced Ag/SiO<sub>2</sub> showed two peaks centered at 367.9 and 373.9 eV, which is typical for the metallic Ag 3d<sub>5/2</sub> and Ag 3d<sub>3/2</sub> (Fig. S11 in the Supporting information), as reported in the literature (367.9–368.1 eV and 373.9–374.1 eV, respectively) [42]. In addition, the Ag 3d<sub>5/2</sub> BE values of Ag<sub>2</sub>O and AgO range from 367.6 eV to 367.7 eV and 367.2 eV to 367.4 eV, respectively [42]. These reports are contrary to the typical positive core level BE shifts of metal cations in ionic materials. As shown in Fig. S10, the Ag 3d<sub>5/2</sub> peak of the as-reduced bimetallic catalysts shifted to relatively higher BE values, as compared with the monometallic Ag/SiO<sub>2</sub> catalyst. These results implied that the Ag species of the bimetallic catalysts had a greater tendency towards electronic richness as compared with those of the monometallic Ag/SiO<sub>2</sub>, according to the anomalous spectral shift of the Ag/Ag<sub>2</sub>O system. However, the positive shift in Ag may also occur due to the smaller size cluster [43].

Given that the Cu<sup>0</sup> and Cu<sup>+</sup> species have almost similar BE values, the XAES spectra was conducted to further discriminate the surface Cu<sup>0</sup> and Cu<sup>+</sup> species of the as-reduced Cu<sub>1</sub>–Ag<sub>x</sub>/SiO<sub>2</sub> catalysts. Asymmetry and overlapping Auger peaks were observed in the XAES spectra of Cu LMM (Fig. 5). These observations strongly indicated that the Cu<sup>0</sup> and Cu<sup>+</sup> species coexisted in the reduced catalysts. The deconvolution results are listed in Table 3. The surface Cu<sup>+</sup> and Cu<sup>0</sup> distributions were significantly affected by the Ag/Cu atomic ratio. The Cu<sup>+</sup>/(Cu<sup>0</sup> + Cu<sup>+</sup>) intensity ratio was initially

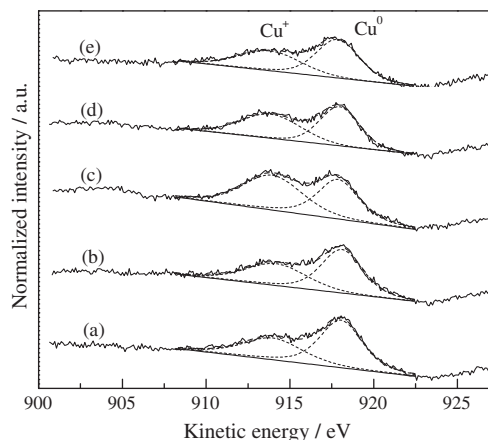


**Fig. 5.** Cu LMM XAES spectra of the as-reduced  $\text{Cu}_1\text{-Ag}_x/\text{SiO}_2$  catalysts with different Ag/Cu atomic ratios. (a)  $\text{Cu}/\text{SiO}_2$ , (b)  $\text{Cu}_1\text{-Ag}_{0.02}/\text{SiO}_2$ , (c)  $\text{Cu}_1\text{-Ag}_{0.05}/\text{SiO}_2$ , (d)  $\text{Cu}_1\text{-Ag}_{0.1}/\text{SiO}_2$ , and (e)  $\text{Cu}_1\text{-Ag}_{0.2}/\text{SiO}_2$ .

enhanced until it reached its maximum value of 53.4% with the Ag/Cu atomic ratio of 0.05, before it was gradually decreased with the further increase in the Ag loading. The Auger parameters (APs) of  $\text{Cu}^0$  and  $\text{Cu}^+$  were close to the previously reported values of 1851.0 and 1847.0 eV, respectively [44].

Based on the XPS data, the surface Ag/Cu ratio was slightly higher than the observed value in the samples with an extremely small amount of Ag, such as  $\text{Cu}_1\text{-Ag}_{0.02}/\text{SiO}_2$  and  $\text{Cu}_1\text{-Ag}_{0.05}/\text{SiO}_2$ . In addition, the surface Ag/Cu ratio was clearly lower than the actual value when that was higher than 0.05. The results verified the possible segregation of the Ag species in bulk particles by STEM-EDS (Fig. S4 in the Supporting information). Nonetheless, the results also demonstrated that Ag species influence the surface Cu NPs, by facilitating contact between Cu and Ag atoms and providing possible synergistic effects.

### 3.2.6. EXAFS

Extended X-ray absorption fine structure (EXAFS) measurements were conducted to further investigate the near-neighbor atomic environment of the Cu and Ag atoms. The Fourier transformations of the Ag K-edge EXAFS spectra of  $\text{Cu}_1\text{-Ag}_{0.05}/\text{SiO}_2$ , Ag/SiO<sub>2</sub>, and Ag foil are shown in Fig. 6. The first nearest neighbor distance of the Ag/SiO<sub>2</sub> was clearly close to that of the Ag foil. The  $\text{Cu}_1\text{-Ag}_{0.05}/\text{SiO}_2$  catalyst showed a relatively broad peak at a position lower than the peak for the Ag foil; this peak of at approximately 0.230 nm was longer than that of Ag<sub>2</sub>O (0.204 nm) [29], thereby implying the existence of an Ag–Cu bond. For the Fourier transformations of the Cu K-edge EXAFS, the first nearest neighbor distance of Cu/SiO<sub>2</sub> and the  $\text{Cu}_1\text{-Ag}_{0.05}/\text{SiO}_2$  catalyst showed no obvious differences from that of the Cu foil (Fig. 7).

**Table 3**  
Cu LMM deconvolution results of  $\text{Cu}/\text{SiO}_2$  and  $\text{Cu}_1\text{-Ag}_x/\text{SiO}_2$  catalysts.

| Catalyst                                    | Ag/Cu atomic ratio | KE <sup>a</sup> (eV) |                 | AP <sup>b</sup> (eV) |                 | Cu 2p <sub>3/2</sub> BE (eV) | X <sub>Cu<sup>+</sup></sub> <sup>c</sup> (%) |
|---|--------------------|----------------------|-----------------|----------------------|-----------------|------------------------------|--|
|   |                    | Cu <sup>+</sup>      | Cu <sup>0</sup> | Cu <sup>+</sup>      | Cu <sup>0</sup> |                              |  |
| $\text{Cu}/\text{SiO}_2$                    | –                  | 914.0                | 918.1           | 1846.5               | 1850.6          | 932.5                        | 38.3   |
| $\text{Cu}_1\text{-Ag}_{0.02}/\text{SiO}_2$ | 0.038              | 914.2                | 918.1           | 1486.9               | 1850.8          | 932.7                        | 40.7   |
| $\text{Cu}_1\text{-Ag}_{0.05}/\text{SiO}_2$ | 0.059              | 914.0                | 917.9           | 1486.8               | 1850.7          | 932.8                        | 53.4   |
| $\text{Cu}_1\text{-Ag}_{0.1}/\text{SiO}_2$  | 0.060              | 913.9                | 918.0           | 1846.8               | 1850.9          | 932.9                        | 46.4   |
| $\text{Cu}_1\text{-Ag}_{0.2}/\text{SiO}_2$  | 0.079              | 913.9                | 917.9           | 1846.8               | 1850.8          | 932.9                        | 40.9   |

<sup>a</sup> Kinetic energy.

<sup>b</sup> Auger parameter.

<sup>c</sup> Intensity ratio between  $\text{Cu}^+$  and ( $\text{Cu}^+ + \text{Cu}^0$ ) by deconvolution of Cu LMM XAES spectra.

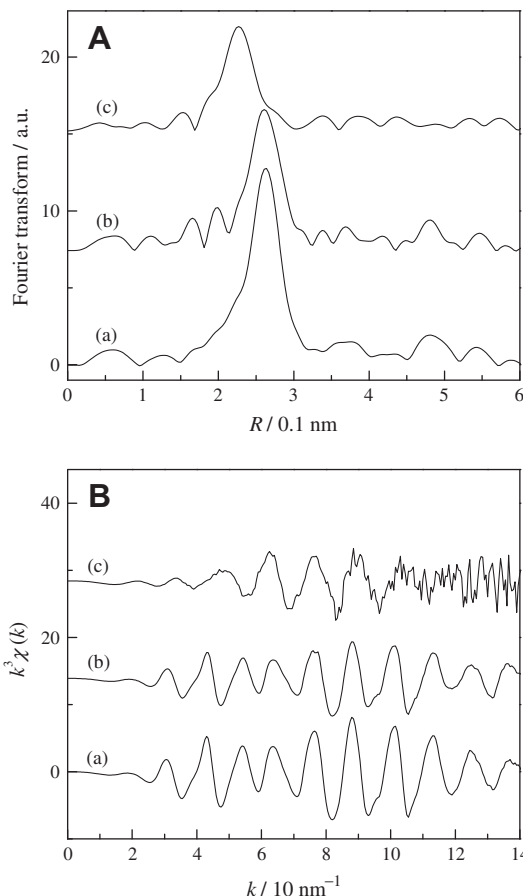


**Fig. 6.** (A) Fourier transforms and (B)  $k^3$ -weighted ( $k$ ) of Ag K-edge EXAFS for (a) Ag foil, (b)  $\text{Ag}/\text{SiO}_2$ , and (c)  $\text{Cu}_1\text{-Ag}_{0.05}/\text{SiO}_2$ .

The structural parameters derived from the EXAFS curve fitting analysis are listed in Table 4 and Table S2. For the Ag K-edge EXAFS of the  $\text{Cu}_1\text{-Ag}_{0.05}/\text{SiO}_2$ , a Cu–Ag shell at a bond distance ( $R$ ) of 0.264 nm with a coordination number ( $N$ ) of 11 was observed without considering the Ag–Ag distance by neglecting the Ag–Ag contribution. When the Ag–Ag coordination was taken into consideration, a Ag–Cu shell at  $R = 0.263$  nm with  $N = 10$  and an Ag–Ag shell at  $R = 0.289$  nm with  $N = 2.7$  were detected. Here, the Ag–Cu coordination number was corrected using the Ag–Ag coordination number because of the absence of a good Ag–Cu reference compound in this study. For the  $\text{Cu}_1\text{-Ag}_{0.05}/\text{SiO}_2$  catalyst, the  $N$  of Ag–Cu was 78% of the total  $N$  of Ag, which suggested that most of the Ag had bonded with Cu to form the Cu–Ag alloy. Additionally, a small part of the Ag (ca. 22%) formed Ag clusters. The much smaller Ag–Ag coordination number of the  $\text{Cu}_1\text{-Ag}_{0.05}/\text{SiO}_2$  ( $N = 2.7$ ), as compared with the Ag foil ( $N = 12$ ), indicated

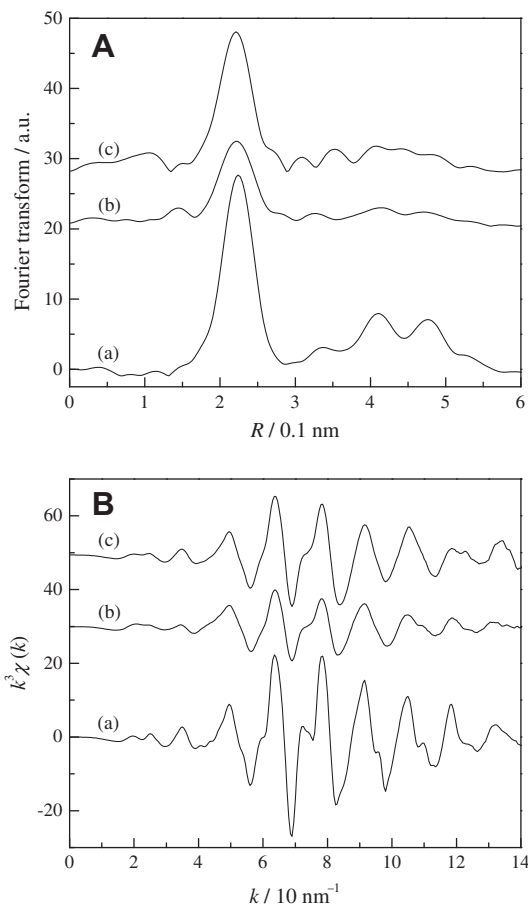


**Fig. 7.** (A) Fourier transforms and (B)  $k^3$ -weighted ( $k$ ) of Cu K-edge EXAFS for (a) Cu foil, (b) Cu/SiO<sub>2</sub>, and (c) Cu<sub>1</sub>-Ag<sub>0.05</sub>/SiO<sub>2</sub>.

**Table 4**

Curve fitting analysis of Ag K-edge EXAFS of Cu<sub>1</sub>-Ag<sub>0.05</sub>/SiO<sub>2</sub>, Ag/SiO<sub>2</sub>, and Ag foil.

| Sample  | Shell | $N^a$ | $R^b$ (nm) | $E^c$ (eV) | $\sigma^d$ (nm) | $R_f^e$ |
|---|-------|-------|------------|------------|-----------------|---------|
| Cu <sub>1</sub> -Ag <sub>0.05</sub> /SiO <sub>2</sub> | Ag-Cu | 11    | 0.264      | 2.2        | 0.0082          | 0.029   |
| Cu <sub>1</sub> -Ag <sub>0.05</sub> /SiO <sub>2</sub> | Ag-Cu | 10    | 0.263      | 1.5        | 0.0076          | 0.012   |
|   | Ag-Ag | 2.7   | 0.289      | 4.1        | 0.0083          |         |
| Ag/SiO <sub>2</sub>                                   | Ag-Ag | 8.9   | 0.285      | 3.6        | 0.0081          | 0.052   |
| Ag foil   | Ag-Ag | 12    | 0.285      | 2.8        | 0.0082          | 0.044   |

<sup>a</sup> Coordination number.

<sup>b</sup> Bond distance between absorber and backscatter atoms.

<sup>c</sup> Inner potential correction to account for the difference in the inner potential between the sample and the reference compound.

<sup>d</sup> Debye-Waller factor.

<sup>e</sup> Residual factor.

the presence of tiny metallic Ag clusters with sizes less than a few nanometers [29]. Moreover, the total  $N$  of Ag was almost 12, thereby indicating that the small Ag cluster was mainly surrounded by

Cu. For the Cu K-edge, the Cu<sub>1</sub>-Ag<sub>0.05</sub>/SiO<sub>2</sub> sample had a Cu-Cu shell at  $R = 0.252$  nm with  $N = 9.2$ . For the Ag content of 0.05 with an Ag-Cu shell of 10, as determined from the Ag K-edge and based on the relation:  $N_{\text{Ag-Cu}} \times C_{\text{Ag}} = N_{\text{Cu-Ag}} \times C_{\text{Cu}}$ , the calculated  $N_{\text{Cu-Ag}}$  was ca. 0.5. This value was too small to be detected. The Cu/SiO<sub>2</sub> sample consisted of a Cu-Cu shell ( $N = 6.2$  at  $R = 0.253$  nm) and a relatively weak Cu-O shell ( $N = 0.8$  at  $R = 0.183$  nm), which implied that the Cu species were somewhat oxidized.

### 3.2.7. Structure-performance relationship

The monometallic Cu/SiO<sub>2</sub> catalyst with relatively low Cu dispersion showed poor catalytic activity and stability. After incorporating a small amount of Ag ( $x \leq 0.05$ ), the bimetallic catalyst exhibited higher Cu dispersion and enhanced catalytic activity and stability. The XRD patterns and TEM images of the catalysts after long-term catalytic test showed that the addition of Ag could effectively suppressed the aggregation of the Cu NPs during the long-term reaction process. Characterizations of EDS, H<sub>2</sub>-TPR, UV-vis DRS, XPS, and XAES revealed that the electronic interactions occurred between Cu and Ag species, as reflected by the fact that the surface Cu<sup>+</sup> and Cu<sup>0</sup> distributions were significantly affected by the Ag/Cu atomic ratio. The Cu<sup>+</sup>/(Cu<sup>+</sup> + Cu<sup>0</sup>) intensity ratio was increased from 38.3% to 53.4% after incorporating 0.65 wt% Ag ( $x = 0.05$ ) to Cu/SiO<sub>2</sub> catalyst. Moreover, the Ag K-edge EXAFS of the Cu<sub>1</sub>-Ag<sub>0.05</sub>/SiO<sub>2</sub> showed that a Ag-Cu shell at  $R = 0.263$  nm with  $N = 10$  and a Ag-Ag shell at  $R = 0.289$  nm with  $N = 2.7$  were detected when the Ag-Ag coordination was taken into account. In other words, the Cu NPs were most probably embedded with Ag nanoclusters. The coherent interactions between Cu NPs and Ag nanoclusters could induce the formation of Cu-Ag alloys during the pretreatment, with important roles for modulating the Cu<sup>+</sup>/Cu<sup>0</sup> ratio and retarding the aggregation of Cu NPs during the reaction process. With the further increase in the Ag/Cu atomic ratio ( $x \geq 0.1$ ), excess Ag nanoclusters would cover or block the surface of Cu NPs, which made the Cu dispersion decreased and the active Cu species inaccessible. Based on the analysis of the structural characterization results, a possible schematic diagram of the Cu<sub>1</sub>-Ag <sub>$x$</sub> /SiO<sub>2</sub> catalysts with varied Ag/Cu atomic ratio is proposed in Fig. 8.

Simultaneous existence of Cu<sup>+</sup> and Cu<sup>0</sup> species on silica-supported Cu-based catalysts has been extensively discussed [3,13,25,45–47]. It is generally accepted that the synergistic effect of Cu<sup>0</sup> and Cu<sup>+</sup> determines the catalytic performance in DMO hydrogenation and a balanced distribution of Cu<sup>+</sup> and Cu<sup>0</sup> is one of the key issues for obtaining outstanding hydrogenation performance [3,13,25,45]. Poels and Brands [46] reported that the Cu<sup>0</sup> species dissociatively adsorbs H<sub>2</sub>, while the Cu<sup>+</sup> species may stabilize the methoxy and the acyl species, which are also important intermediates in the hydrogenation of DMO. Moreover, Cu<sup>+</sup> species may function as electrophilic or Lewis acid sites to polarize the C=O bond via the electron lone pair on oxygen [3,25], thus improving the reactivity of the ester group in DMO.

The cooperative effect of Cu<sup>0</sup> and Cu<sup>+</sup> species is inevitably believed to influence the catalytic performance of Cu<sub>1</sub>-Ag <sub>$x$</sub> /SiO<sub>2</sub>

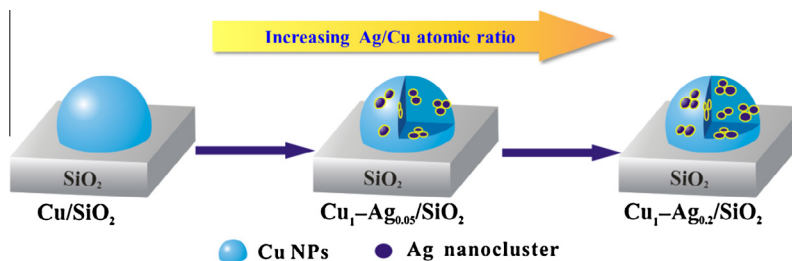


**Fig. 8.** Schematic diagram of Cu<sub>1</sub>-Ag <sub>$x$</sub> /SiO<sub>2</sub> catalysts with different Ag/Cu atomic ratios.

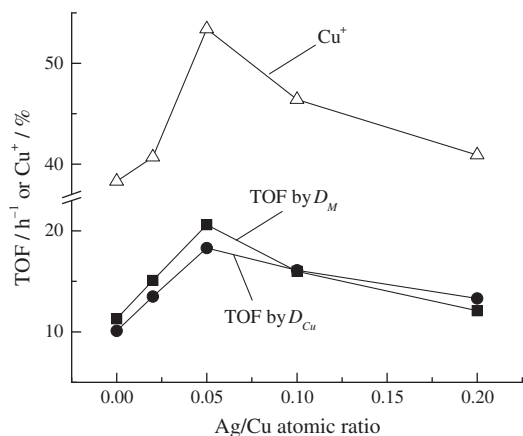


Fig. 9. TOF and  $Cu^+/(Cu^0 + Cu^+)$  intensity ratio as a function of the Ag/Cu atomic ratio.

catalysts. By combining the catalytic results with the Cu and metal dispersion, as well as the  $Cu^+/Cu^0$  ratio, the effects of Ag/Cu atomic ratio and the  $Cu^+/Cu^0$  ratio on the TOF can be discussed with respect to the number of surface metal atoms. The  $Cu^+/(Cu^0 + Cu^+)$  intensity ratio and TOF both showed a volcano-type dependence on the Ag/Cu atomic ratio (Fig. 9). The  $Cu^+/(Cu^0 + Cu^+)$  ratio and TOF value were proportionally increased with Ag content when the Ag/Cu atomic ratio was less than 0.05. The  $Cu^+/(Cu^0 + Cu^+)$  ratio and TOF value simultaneously reached their summits in the case of Ag/Cu atomic ratio at 0.05. After that, both were decreased gradually. Thus, besides the coverage or blockage of Cu NPs by excess Ag, the balanced  $Cu^+/(Cu^0 + Cu^+)$  ratio was disturbed with relative high content of surface Ag species, resulting in the decrease in catalytic performance. The results likewise demonstrate that the hydrogenation of DMO is a structure-sensitive reaction. Consequently, adding the appropriate amount of Ag can be an effective way to modulate the proportion of surface  $Cu^+$  and  $Cu^0$  to obtain excellent activity and stability for the hydrogenation of DMO.

#### 4. Conclusions

The incorporation of an appropriate amount of Ag into  $Cu/SiO_2$  was significantly demonstrated to enhance the catalytic activity and stability for the hydrogenation of DMO to EG. The EG yield over the optimized catalyst  $Cu_1-Ag_{0.05}/SiO_2$  was 2.2 times higher, as compared with the monometallic  $Cu/SiO_2$  at 463 K and 3.0 MPa, with a  $H_2/DMO$  molar ratio of 80, and a  $WLHSV_{DMO}$  of  $1.05 h^{-1}$ . The  $Cu_1-Ag_{0.05}/SiO_2$  catalyst can maintain almost 100% DMO conversion and more than 97% EG selectivity for over 150 h under the optimized conditions.

A series of spectroscopic studies were used to explore the structure of the catalysts, including  $N_2O$  chemisorption, TEM, *in situ* XRD, EDS,  $H_2$ -TPR, UV-vis DRS, XPS, XAES, and EXAFS. Introducing the appropriate amount of Ag facilitates the higher dispersion of Cu NPs. This higher dispersion is caused by the formation of Cu NPs containing Ag nanoclusters. The coherent interactions between the Cu and Ag species induce the formation of Cu–Ag alloys. The distribution of surface  $Cu^+$  and  $Cu^0$  species can be modulated by varying the Ag/Cu atomic ratio. Therefore, the interactions between Cu and an appropriate amount of Ag species can help sustain a suitable  $Cu^+/Cu^0$  proportion and restrain the transmigration of copper NPs, which are largely responsible for

the excellent activity and stability of the bimetallic Cu–Ag/ $SiO_2$  catalyst.

#### Acknowledgments

We gratefully acknowledge the financial support from the National Basic Research Program of China (2011CBA00508), the Natural Science Foundation of China (20923004 and 21173175), the Research Fund for the Doctoral Program of Higher Education (20110121130002), the Program for Changjiang Scholars and Innovative Research Team in University (IRT1036), and Cooperative Research Program of Catalysis Research Center, Hokkaido University (Grant No. 10B0043).

#### Appendix A. Supplementary material

Supplementary data associated with this article can be found, in the online version, at <http://dx.doi.org/10.1016/j.jcat.2013.07.006>.

#### References

- [1] H.L. Yue, Y.J. Zhao, X.B. Ma, J.L. Gong, Chem. Soc. Rev. 41 (2012) 4218.
- [2] R.A. Kerr, R.F. Service, Science 309 (2005) 101.
- [3] L.F. Chen, P.J. Guo, M.H. Qiao, S.R. Yan, H.X. Li, W. Shen, H.L. Xu, K.N. Fan, J. Catal. 257 (2008) 172.
- [4] G.H. Xu, Y.C. Li, Z.H. Li, H.J. Wang, Ind. Eng. Chem. Res. 34 (1995) 2371.
- [5] Z.N. Xu, J. Sun, C.S. Lin, X.M. Jiang, Q.S. Chen, S.Y. Peng, M.S. Wang, G.C. Guo, ACS Catal. 3 (2013) 118.
- [6] D.S. Brands, E.K. Poels, A. Bliet, Appl. Catal. A: Gen. 184 (1999) 279.
- [7] L.R. Zehner, R.W. Lenton, US Patent 4 112 245, 1978.
- [8] F. Poppelsdorf, Eur. Patent 0 060 787, 1982.
- [9] S. Tahara, K. Fujii, K. Nishihira, M. Matsuda, K. Mizutare, US Patent 4 453 026, 1984.
- [10] K. Hirai, T. Uda, Y. Nakamura, US Patent 4 614 728, 1986.
- [11] H. Miyazaki, K. Hirai, T. Uda, Y. Nakamura, S. Ikezawa, T. Tsuchie, US Patent 57 122 946, 1982.
- [12] H. Miyazaki, T. Uda, K. Hirai, Y. Nakamura, H. Ikezawa, T. Tsuchie, US Patent 4 585 890, 1986.
- [13] Z. He, H.Q. Lin, P. He, Y.Z. Yuan, J. Catal. 277 (2011) 54.
- [14] H.Q. Lin, X.L. Zheng, Z. He, J.W. Zheng, X.P. Duan, Y.Z. Yuan, Appl. Catal. A: Gen. 445–446 (2012) 287.
- [15] A.Y. Yin, C. Wen, X.Y. Guo, W.L. Dai, K.N. Fan, J. Catal. 280 (2011) 77.
- [16] C. Wen, Y.Y. Cui, A.Y. Yin, K.N. Fan, W.L. Dai, ChemCatChem 5 (2013) 138.
- [17] A.Y. Yin, X.Y. Guo, K.N. Fan, W.L. Dai, ChemCatChem 2 (2010) 206.
- [18] Y.Y. Zhu, S.R. Wang, L.J. Zhu, X.L. Ge, X.B. Li, Z.Y. Luo, Catal. Lett. 135 (2010) 275.
- [19] L. Lin, P.B. Pan, Z.F. Zhou, Z.J. Li, J.X. Yang, M.L. Sun, Y.G. Yao, Chin. J. Catal. 32 (2011) 957.
- [20] S.R. Wang, X.B. Li, Q.Q. Yin, L.J. Zhu, Z.Y. Luo, Catal. Commun. 12 (2011) 1246.
- [21] S.R. Wang, L.J. Zhu, Y.Y. Zhu, X.L. Ge, X.B. Li, Chin. Chem. Lett. 22 (2011) 362.
- [22] C. Wen, A.Y. Yin, Y.Y. Cui, X.L. Yang, W.L. Dai, K.N. Fan, Appl. Catal. A: Gen. 543 (2013) 82.
- [23] X.Y. Guo, A.Y. Yin, W.L. Dai, K.N. Fan, Catal. Lett. 132 (2009) 22.
- [24] A.Y. Yin, X.Y. Guo, W.L. Dai, H.X. Li, K.N. Fan, Appl. Catal. A: Gen. 349 (2008) 91.
- [25] A.Y. Yin, X.Y. Guo, W.L. Dai, H.X. Li, K.N. Fan, J. Phys. Chem. C 113 (2009) 11003.
- [26] A.Y. Yin, X.Y. Guo, W.L. Dai, K.N. Fan, J. Phys. Chem. C 114 (2010) 8523.
- [27] C.L. Bracey, P.R. Ellis, G.J. Hutchings, Chem. Soc. Rev. 38 (2009) 2231.
- [28] X.Y. Liu, A.Q. Wang, L. Li, T. Zhang, C.Y. Mou, J.F. Lee, J. Catal. 278 (2011) 288.
- [29] K. Shimizu, K. Shimura, M. Nishimura, A. Satsuma, RSC Adv. 1 (2011) 1310.
- [30] J.X. Zhou, L.Y. Guo, X.W. Guo, J.B. Mao, S.G. Zhang, Green Chem. 12 (2010) 1835.
- [31] J.W. Zheng, H.Q. Lin, Y.N. Wang, X.L. Zheng, X.P. Duan, Y.Z. Yuan, J. Catal. 297 (2012) 110.
- [32] A. Sandoval, A. Aguilar, C. Louis, A. Traverse, R. Zanella, J. Catal. 281 (2011) 40.
- [33] A.Y. Yin, C. Wen, W.L. Dai, K.N. Fan, J. Mater. Chem. 21 (2011) 8997.
- [34] Y.N. Wang, X.P. Duan, J.W. Zheng, H.Q. Lin, Y.Z. Yuan, H. Ariga, S. Takakusagi, K. Asakura, Catal. Sci. Technol. 2 (2012) 1637.
- [35] B.W. Wang, Q. Xu, H. Song, G.H. Xu, J. Nat. Gas Chem. 16 (2007) 78.
- [36] J.R. Anderson, Structure of Metallic Catalysts, Academic Press, New York, 1975.
- [37] T. Furusawa, K. Seshan, J.A. Lercher, L. Lefferts, K. Aika, Appl. Catal. B: Environ. 37 (2002) 205.
- [38] J.J.F. Scholten, J.A. Konvalinka, F.W. Beekman, J. Catal. 28 (1973) 209.
- [39] C.J.G. Van Der Grift, A. Mulder, J.W. Geus, Appl. Catal. 60 (1990) 181.
- [40] H.T. Beyene, V.S.K. Chakravadhanula, C. Hanisch, T. Strunskus, V. Zaporozhchenko, M. Elbahri, F. Faupel, Plasmonics 7 (2012) 107.
- [41] U. Kreibitz, M. Vollmer, Optical Properties of Metal Clusters, Springer, Berlin, 1995.

- [42] C.D. Wagner, W.M. Riggs, L.E. Davis, J.F. Moulder, in: G.E. Muilenberg (Ed.), *Handbook of X-ray Photoelectron Spectroscopy*, Perkin-Elmer, Physical Electronics Division, Eden Prairie, Minnesota, 1979.
- [43] M.G. Mason, *Phys. Rev. B* 27 (1983) 748.
- [44] K.P. Sun, W.W. Lu, F.Y. Qiu, S.W. Liu, X.L. Xu, *Appl. Catal. A: Gen.* 252 (2003) 243.
- [45] J.L. Gong, H.R. Yue, Y.J. Zhao, S. Zhao, L. Zhao, J. Lv, S.P. Wang, X.B. Ma, *J. Am. Chem. Soc.* 134 (2012) 13922.
- [46] E.K. Poels, D.S. Brands, *Appl. Catal. A: Gen.* 191 (2000) 83.
- [47] V. Gutierrez, M. Dennehy, A. Diez, M.A. Volpea, *Appl. Catal. A: Gen.* 437 (2012) 72.